General Disclaimer

One or more of the Following Statements may affect this Document

- This document has been reproduced from the best copy furnished by the organizational source. It is being released in the interest of making available as much information as possible.

- This document may contain data, which exceeds the sheet parameters. It was furnished in this condition by the organizational source and is the best copy available.

- This document may contain tone-on-tone or color graphs, charts and/or pictures, which have been reproduced in black and white.

- This document is paginated as submitted by the original source.

- Portions of this document are not fully legible due to the historical nature of some of the material. However, it is the best reproduction available from the original submission.

AN APPLICATION OF OVERSET GRIDS TO PAYLOAD/FAIRING THREE-DIMENSIONAL INTERNAL FLOW CFD ANALYSIS

M. Kandula* and R. Nallasamy
ASRC, Kennedy Space Center, FL 32899 USA

P. Schallhorn and L. Duncil
NASA Kennedy Space Center, FL 32899 USA

* E-Mail: Max.Kandula-1@ksc.nasa.gov(Corresponding Author)

ABSTRACT

The application of overset grids to the computational fluid dynamics analysis of three-dimensional internal flow in the payload/fairing of an expendable launch vehicle is described. In conjunction with the overset grid system, the flowfield in the payload/fairing configuration is obtained with the aid of OVERFLOW Navier-Stokes code. The solution exhibits a highly three dimensional complex flowfield with swirl, separation, and vortices. Some of the computed flow features are compared with the measured Laser-Doppler Velocimetry (LDV) data on a $1/5^{th}$ scale model of the payload/fairing configuration. The counter-rotating vortex structures and the location of the saddle point predicted by the CFD analysis are in general agreement with the LDV data. Comparisons of the computed (CFD) velocity profiles on horizontal and vertical lines in the LDV measurement plane in the faring nose region show reasonable agreement with the LDV data.

Keywords: chimera overset grids, payload fairing, turbulence models, Navier-Stokes solutions, internal flow

1. INTRODUCTION

Overset (or embedded) grids are increasingly considered in the CFD applications for the prediction of flowfield about complex three dimensional geometries. In the well-known chimera overset grid scheme (Benek et al. 1986) overlapping grids are generated about individual (component) grids, and intergrid boundary communication is accomplished through interpolation. It does not require common boundaries as in the case of patched grids. It thus affords great geometric flexibility and independence (different grid topologies) and also permits different flow models (turbulence models, gas models, such as perfect gas and real gas, and algorithms) to be considered in the component subdomains constituting the overall grid system.

Overlapping grids were mostly applied to problems of high speed aerodynamics. These include space shuttle external flow (Slotnik et al. 1994), and numerous aircraft and missile configurations. The reported applications of overset grids to low speed internal flows are, however, relatively few.

The present paper reports the application of an overset grid method for the computation of low-speed three-dimensional internal flow past a spacecraft encapsulated within a payload/fairing of a Delta II expendable launch vehicle (ELV). A primary objective of this work is to develop CFD models for simulating prelaunch air flowfield within the payload fairing. The flow solution is obtained with the OVERFLOW code (Kandula and Buning 1994, Pulliam 1997, Buning et al. 1998) which solves the Navier-Stokes equations with one- or two-equation turbulence models. The computed flow

features and velocity profiles are compared with the measured Laser Doppler velocimetry (LDV) data acquired on a 1/5 scale model on the payload fairing configuration.

2. PAYLOAD FAIRING ANALYSIS

2.1 Geometric Configuration

The payload fairing (PLF) of an expendable launch vehicle encapsulates the spacecraft and protects the payload by shielding it from aerodynamic buffeting and heating while in the lower atmosphere , and also from vibroacoustic loading during the launch phase. A typical PLF consists of a cone/cylinder structure, biconic section, conditioning air diffuser, acoustic absorption blankets, and fairing separation system. The payload fairing is jettisoned off as soon as the launcher leaves the atmosphere. Prior to launch, the payload is cooled by circulating cold air delivered through an air conditioning (AC) pipe attached to the fairing from the outside. The conditioned air flows past a diffuser located at the pipe/fairing interface. After passing over the spacecraft mounted within the fairing, it is finally discharged. The PLF air conditioning is cut off at lift-off.

The payload/fairing considered here is the 10C/ (EO-1 & SAC-C) fairing that encapsulates two spacecrafts, an Earth-Observation satellite (EO-1) and the Satellite de Applications Centificas-C (SAC-C) with a Dual Payload Attach Fitting (DPAF). It has a cylindrical type structure with conical ends. The EO-1 is attached on the top of the DPAF and the SAC-C is installed inside the cylindrical portion of the DPAF. Here only the EO-1 spacecraft is modeled. The EO-1 has a hexagonal base on which various components are mounted (figure1). The major components include the hexagonal main structure, Advanced Land Imager (ALI), Hyperion, X-band boom, and solar arrays (figure 2). Some of the computational aspects of the internal flow of this payload/fairing pre-launch air

cooling system have been described in Kandula and Walls (2003). Detailed descriptions of the test model, LDV measurement system, seeding, and test procedure were presented in Kandula et al (2005).

2.2 Grid generation

2.2.1 Geometric simplifications

Practical considerations in the construction of a reasonable grid system for CFD analysis of complex configurations require some essential geometric simplifications. In the present context, these simplifications include the identification of major spacecraft components that are attached to the main structure, which in our judgment have significant effects on the overall flowfield. Factors such as volume, surface area, and relative geometric orientation have obvious impacts in this consideration. Components having admittedly lesser influence were altogether ignored. Also, for a given component, some minor approximations to the surface shape were also considered. The overall objective in the simplification process is to balance the number of grid points (computational cost and grid generation time) vis-à-vis the solution accuracy.

2.2.2 Overlapping scheme

Overlapping grids are generated for the entrance AC pipe, fairing, and spacecraft. Various grid topologies are considered including O-grid and H-grid. In the intersection regimes, such as pipe/fairing and spacecraft main structure component intersections, collar grids were considered. The collar grids provide the communication between the intersecting grids, as well as necessary resolution for viscous flow computation. Surface grids for the components are generated primarily with the Gridgen code (Steinbrenner and Chawner 2005). The collar surface grids are built with the well-known Chimera Grid

Tools, which include HYPGEN hyperbolic grid generation package (Chan et al. 1999). A more detailed discussion on the collar grids may be found in Parks et al (1991). Field (volume) grids are obtained from Gridgen and HYPGEN. Intergrid boundary communication is obtained with the aid of PEGASUS software (Suhs and Tramel 1991).

2.2.3 Primary Grids

The primary grids (excluding the collar grids) are first generated as described above. Figure 3 displays the surface grids for the PLF and the EO-1. An O-grid is employed for AC pipe, with an axis boundary condition, as seen in figure 4(a). An H-grid is considered for the PLF volume grid, as indicated in figure 4(b). A single grid is created for the EO-1 and the DPAF, with an axis boundary condition at the hexagonal end. The surface grid for EO-1/DPAF is indicated in figure 4. The diffuser grid is composed of two axis boundary conditions.

2.2.4 Collar Grids

a. Fairing/pipe collar grid

The generation of fairing/pipe collar grid for internal flow is somewhat analogous to that of exterior grids such as in wing/fuselage junction of an aircraft grid system. But the present case of internal flow leads to considerable complexity. The process of grid generation for the collar volume grid is summarized as follows. Starting from the intersection curve of the fairing/pipe surfaces, surface grids were grown on the pipe and the fairing. From the outer edge (boundary) of the surface grid on the fairing interior surface, a cylindrical type surface grid is grown normal to the wall so that it protrudes into the fairing interior to some distance from the wall.

Figure 5 shows the surface grid of the collar, which is composed of the surface grid on the pipe, surface grid on the fairing, and the flow-through extension into the fairing interior. From the surface grid, an interior volume grid for the collar is developed with the aid of GRIDGEN software. Initial volume grids were built with the algebraic transfinite interpolation. These grids were smoothed by running the three dimensional elliptic solver. To the authors' knowledge, such an internal collar grid generation has not been reported previously.

b. Spacecraft collar grids

Five collar grids are required for the EO-1 spacecraft modeling. One main observation is that the initial surface grid for the main spacecraft structure needs to be locally refined when inserting the collar grids. This crucial step is necessary for carrying out the PEGSUS interpolation.

2.2.5 Intergrid Communication

In the overlapping grid system, grids are chosen to cut holes in other grids, and to overlap any number of grids. The interpolation process in PEGASUS code is briefly described here with the aid of figure 6 in which the solid boundary of mesh 2 intersects mesh 1(see Rogers et al. 2003). Grid points in mesh 1 that are inside the solid body of mesh 2 are blanked out, and are known as hole points, which are excluded from the computational domain. The grid points in mesh 1 surrounding the blanked points, known as hole-fringe points, receive flowfield information interpolated from grid points in mesh 2. The grid points on the outer boundary of mesh 2 obtain flowfield information interpolated from grid points in mesh 1.

The PEGASUS code provides the interpolation data required by the flow solver for the inter-grid communication. The output typically consists in a list of the mesh points that are interpolated, the donor cells for each interpolated point, and a list of blanked out points (hole points).

2.2.6 Overall Grid System

The overall grid system for the 10C/EO-1 is composed of 12 grids and 2.5×10^6 grid points. This grid system includes grids for fairing, AC pipe, pipe/fairing collar, diffuser, EO-1, solar array, ALI, Hyperion, X-band boom and collar grids for the intersections of ALI, Hyperion, and X-band boom with the EO-1.

2.3 Flow solution

The steady flowfield solution is obtained using the OVERFLOW code (Kandula and Buning 1994, Jespersen et al. 1997). OVERFLOW code is a three-dimensional Navier-Stokes code developed by NASA. It solves the governing mean flow equations in conservation form in generalized coordinates (ξ, η, ζ) that are transformations of the rectangular coordinate space (x, y, z). The compressible Navier-Stokes equations that are solved in OVERFLOW are of the form

$$(Q/J)_t + E_\xi + F_\eta + G_\zeta = \mathrm{Re}^{-1}\left(F_{v\xi} + G_{v\eta} + H_{v\zeta}\right) \tag{1a}$$

where the solution vector Q containing conservative variables is defined by

$$Q = (\rho, \rho u, \rho v, \rho w, e)/J \tag{1b}$$

Here J is the geometric transformation Jacobian, F, G and H are inviscid fluxes, and F_v, G_v, and H_v are the viscous fluxes.

The present solutions are based on the diagonalized version of the Beam-Warming three-factor approximate factorization scheme (Beam and Warming, 1976), with central

differencing for convective fluxes and diffusion fluxes. Although incompressible CFD codes are available, OVERFLOW code was chosen here because of its well tested Chimera grid handling capability. Low Mach number preconditioning is employed for the present investigation to accelerate convergence.

2.3.1 Turbulence model

The validity of CFD analysis is critically dependent on the choice of turbulence model. Two-equation models provide better flow physics than one-equation models with regard to adverse pressure gradients, flow separation, etc. (Kandula and Wilcox 1995). However, for practical application involving three-dimensional (3-D) flows, one-equation models are frequently considered (e.g., Space Shuttle ascent flowfield, Slotnik et al. 1994), since two-equation models and higher-order models are cost-prohibitive despite their ability to include improved flow physics.

Both one- and two-equation turbulence models are implemented in the code. The one-equation turbulence models include those of Spalart-Allmaras (1992) and Baldwin and Barth (1980), and the two-equation models include that of $k-\omega$ Shear Stress Transport (SST) model due to Menter (1994). However, only one equation turbulence models are considered here. The Spalart-Allmaras (1992) one equation turbulence model, which is widely considered in external aerodynamics, is chosen as the base-line model for this application. In this method, a single partial differential equation for the transport of turbulence kinetic energy, k is solved for. This model is widely considered and validated for different flow regimes.

2.3.2 Initial and boundary conditions

The flow starts from rest at $t = 0$ in the entire system. Appropriate boundary conditions were imposed, including the solid wall, inflow and outflow boundary conditions. Inflow velocity profile and mass flow rate are specified at the pipe inlet. The static pressure at the outflow boundary was adjusted to get the necessary mass flow rate. Convergence is achieved using time-stepping scheme, multi-grid cycling, and low Mach number preconditioning.

2.3.3 Flow conditions

Steady state solution for this grid system was obtained for a pipe Reynolds number of 2.40×10^5 (based on pipe diameter) and a Mach number of 0.04. This Reynolds number corresponds to full scale model with an air conditioning pipe of 10 inch (25.4 cm) diameter.

In the second phase of the work, a $1/5^{th}$ scale model of the payload/faring was built and Laser Doppler Velocimeter (LDV) measurements were made. For dynamic similarity, the Reynolds number in the scale model should be the same as in the prototype (full-scale) model. However, due to difficulties with the particle seeding with the olive oil in the model test, the flow rate had to be reduced by a factor of 4. Thus the model testing and CFD comparisons were done at $1/4^{th}$ of the full scale Reynolds number, i.e., 0.593×10^5. The details of the model and the experimental procedure are discussed in Kandula et al. (2005).

3. RESULTS AND DISCUSSIONS

3.1 Full-scale Reynolds number solution

3.1.1 Convergence History

Figure 7 shows the convergence history for the solution residuals. This residual history serves as a qualitative measure of convergence to the steady state and suggests that convergence is approached in about 2000 iterations. A quantitative measure of convergence is provided by the convergence history of the ratio of the exit to inlet mass flow rate, as shown in figure 8.

3.1.2 Flowfield solution

An examination of the steady state flowfield suggests that the flow is highly three dimensional and is characterized by swirling flow, vortex flow, and separated flow. The streak lines (neutrally buoyant marker path lines) originating from the pipe outlet are displayed in figure 9(a). Figure 9(b) shows calculated streak lines from a source located on EO-1. It is seen that these streak lines negotiate limited upstream movement and eventually exit downstream. The streak lines demonstrate complicated three-dimensional swirling flow.

Velocity vectors over the EO-1 surface, shown in figure 10(a) suggest that flow separation is noted on the EO-1/DPAF intersection region and on downstream end of the DPAF. Reattachment of the flow occurs at the downstream end of the guidance section. Figure 10(b) exhibits the velocity vectors in the cross section of the fairing corresponding to an axial plane. Secondary flow, characteristics of swirl flow, is evident from this plot.

3.2 Test Reynolds number solution

3.2.1 LDV Measurements

A $1/5^{th}$ scale model of the payload/fairing was built, shown in figure 11, and the test data for the velocity field was obtained from the scale model test. Gaseous Nitrogen (GN2), serving as the test fluid, was supplied from a tube bank at 2400 psig and the pressure was reduced by pressure regulators.

Laser Doppler Velocimetry (LDV) was used to obtain planar (two dimensional) velocity measurements. An Ar-Ion continuous wave laser was employed in backscatter mode. The laser had a 60 mW power in each wavelength of measurement 486 nm and 514 nm. Each of the two colors is used to measure one velocity component. The Burst Spectrum Analyzer (BSA) can provide up to 100,000 velocity measurements per sec. Three dimensional laser traverse system had a range of 310 mm x 310 mm. Form a built in software, a Cartesian mesh with the desired resolution was defined for the plane of measurement.

Olive oil was used as the seeding particle. The SCITEK seeder produced olive oil droplets with the mean droplet diameter of about 2 to 3 μm. Problems were encountered because of low particle seeding level and condensation of moist air on the outside of the model. At the normal flow rate of 22 lbm/min (9.97 kg/min), the seeding was found to be inadequate as the sampling rate was unacceptably low. A decision was therefore made to reduce the flow rate by a factor of 4 (Reynolds number is reduced by a factor of 4). This afforded a good sampling rate of about 1000 samples/sec. Thus the test operation is at a lower Reynolds number than that of the full scale Reynolds number. Hence an additional

CFD solution was obtained for the reduced Reynolds number of 0.593×10^5 for validation with the LDV data.

The CFD and LDV data comparisons in the present paper, is limited to a measurement plane shown in figure 12. This measurement plane is located in the fairing nose region and is oriented at about 6 degrees from the pipe axis.

3.2.2 Comparison of CFD with LDV measurements

As mentioned above, the scale model LDV tests were conducted at a Reynolds number of 0.593×10^5, which is $1/4^{th}$ of that of the full-scale. At this low Reynolds number considerable convergence difficulties were experienced. From the steady state solutions, the velocity fields on the measurement plane were interpolated using Tecplot software. The velocity profiles on specified horizontal and vertical lines in the measurement plane were also interpolated from CFD solutions and LDV data.

Figures 13(a) and 13(b) show the velocity vectors from CFD solution and LDV data respectively in the measurement plane. In these plots, the quantities x and z' corresponds to axial (longitudinal) and transverse coordinates respectively. The CFD solution is obtained at a freestream turbulence Reynolds number $\mathrm{Re}_t = 0.01$. The CFD solution predicts two vortex structures of opposite sign and one saddle point (where the velocity magnitude vanishes). These represent topological information of the velocity vector field. Measurements have captured only the saddle point, while the vortices are not defined clearly and entirely due to measurement difficulties. The saddle point location (z' = -3 inches and x = 8 inches) predicted by the CFD agrees with the LDV data.

The velocity profiles at constant x stations (x = 7, 8.5, 9 and 11 inches) are shown in figure 14. Only for a limited range of z' values, the computed velocity profiles for

both u_x and $u_{z'}$ agree with the LDV data. This is primarily attributed to the difficulty of measurements near the curved walls of the fairing nose. The velocity profiles at constant z' planes (z' = -5, -3, -2, and 0 inches) are shown in figure 15. In these profiles it is seen that the velocity component u_x agrees satisfactorily with the LDV data while the $u_{z'}$ component shows substantial differences.

4. CONCLUSIONS

Overlapping grid technology is shown to predict the low speed three-dimensional internal flow characteristics of the payload/fairing. Complex flow patters were observed. The flow is highly three dimensional, and is characterized by swirling flow, vortex flow, and separated flow.

The solution corresponding to the model test Reynolds number predicts the vortex system indicated by the LDV measurements. The predicted location of the saddle point agrees with that of the LDV data. The velocity profiles in the measurement plane show reasonable agreement with the experimental data for the axial velocity component, but discrepancies exist for the transverse velocity component...

ACKNOWLEDGEMENTS

This work was supported by the Launch Services Program (LSP) at Kennedy Space Center.

REFERENCES

1. Baldwin BS and Barth TJ (1980). A one-equation turbulence transport model for high Reynolds number wall-bounded flows, NASA-TM-102847.

2. Beam R and Warming RF (1976). An implicit finite difference algorithm for hyperbolic systems in conservation law form, *J. Comput. Phys.* 22:87-110.

3. Benek JA, Steger JL, Dougherty FC and Buning PG 1986). Chimera- A grid embedding technique, AEDC-TR-85-64, Arnold Engineering Development Center, Tennessee.

4. Buning PG. et al. (1998). OVERFLOW User's Manual, Version 1.8s, NASA Langley Research Center, Moffett Field, California.

5. Chan WM, Rogers SE, Nash SM, and Buning PG. (1999). Users manual for Chimera grid tools (Version 1.0), NASA Ames Research Center, Moffett Field, California.

6. Jespersen D, Pulliam TH and Buning PG (1997). Recent enhancements to OVERFLOW code, AIAA-97-0644.

7. Kandula M and Buning PG (1994). Implementation of LU-SGS algorithm and Roe upwinding scheme in OVERFLOW thin layer Navier-Stokes code, 25th AIAA Fluid Dynamics Conference, AIAA-94-2357.

8. Kandula M, Hammad K and Schallhorn P. (2005). CFD validation with LDV test data for payload/fairing internal flow, AIAA-2005-4910.

9. Kandula M and Walls L (2003). An application of Overset grids to payload/fairing internal flow CFD analysis, AIAA-2002-3253.

10. Kandula M and Wilcox DC (1995). An examination of $k-\omega$ turbulence model for boundary layers, free shear layers and separated flows, AIAA-95-2317.

11. Menter FR (1994). Two-equation eddy viscosity turbulence model for engineering applications, *AIAA J* 32:1598-1605.

12. Parks SJ, Buning PG, Steger JL and Chan WM (1991). Collar grids for intersecting geometric components within the Chimera overlapped grid scheme, AIAA-91-3423.

13. Rogers SE, Suhs NE and Dietz WE (2003). PEGASUS 5: An automated preprocessor for overset-grid computational fluid dynamics, *AIAA J* 41:1037-1045.

14. Shames I (1982). Mechanics of Fluids, 2nd Edition. McGraw-Hill, New York.

15. Slotnik JP, Kandula M and Buning PG (1994). Navier-Stokes simulations of the space shuttle launch vehicle flight transonic flowfield using large scale Chimera grid system, AIAA-94-1860.

16. Spalart PR and Allmaras SR (1992). A one equation turbulence model for aerodynamic flows, AIAA-92-0439.

17. Steinbrenner J and Chawner JR (1994). The Gridgen Version-9 Multiple block grid generation software, MDA Engineering Report 94-01.

18. Suh NE and Tramel RW (1991). Pegsus 4.0 User's manual, Arnold Engineering development center, AEDC-TR-91-8, Arnold Air force Base, Tennessee.

FIGURE CAPTIONS

Fig. 1 Schematic of the payload fairing geometry

Fig. 2 Payload components description

Fig. 3 Surface grids for a) fairing and b) EO-1

Fig. 4 Volume grids for a) pipe, b) fairing

Fig. 5 Pipe/fairing collar grid development

Fig. 6 Illustration of intergrid communication and interpolation in the PEGASUS code (adapted from Rogers et al. 2003)

Fig. 7 Residual convergence history

Fig. 8 Mass flow rate convergence history

Fig. 9(a) Streak lines emanating from the pipe/fairing collar

Fig. 9(b) Typical source streak lines

Fig. 10(a) Velocity vectors on the EO-1

Fig. 10(b) Velocity vectors in the cross sectional plane of the fairing downstream of the hexagonal structure

Fig. 11 Schematic of the payload/fairing test section (1/5 scale model)

Fig. 12 LDV Measurement plane locations: two views

Fig. 13 Velocity vectors in the measurement plane (a) CFD (b) LDV data

Fig. 14 Velocity profiles at constant x

Fig. 15 Velocity profiles at constant z'

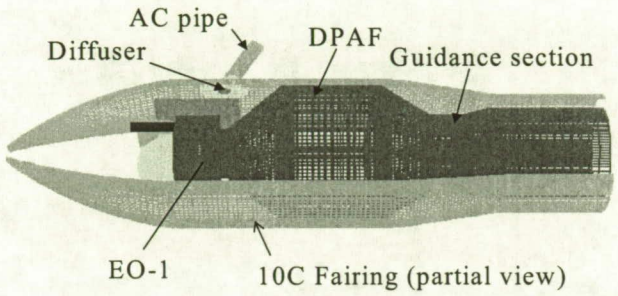

Fig. 1 Schematic of the payload/fairing geometry

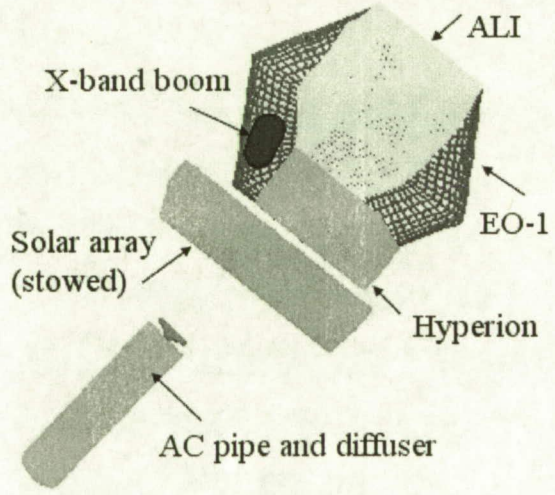

Fig. 2 Payload components description

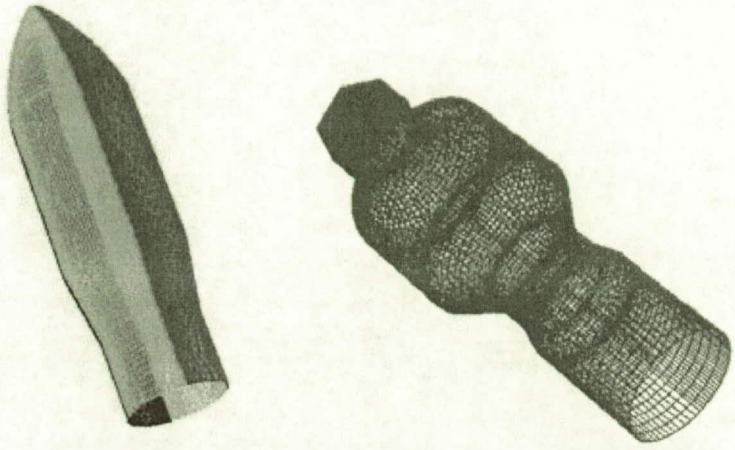

Fig. 3 Surface grids for a) fairing and b) EO-1

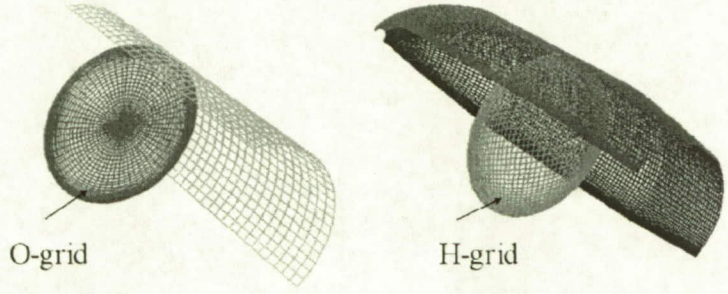

Fig. 4 Volume grids for a) pipe, b) fairing

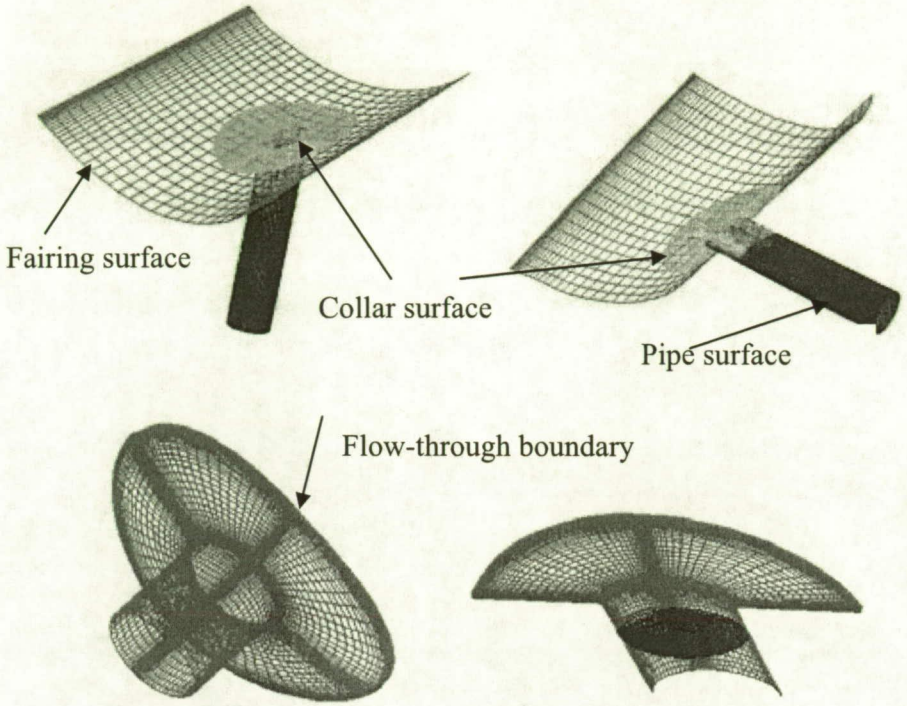

Fig 5 pipe/fairing collar grid development

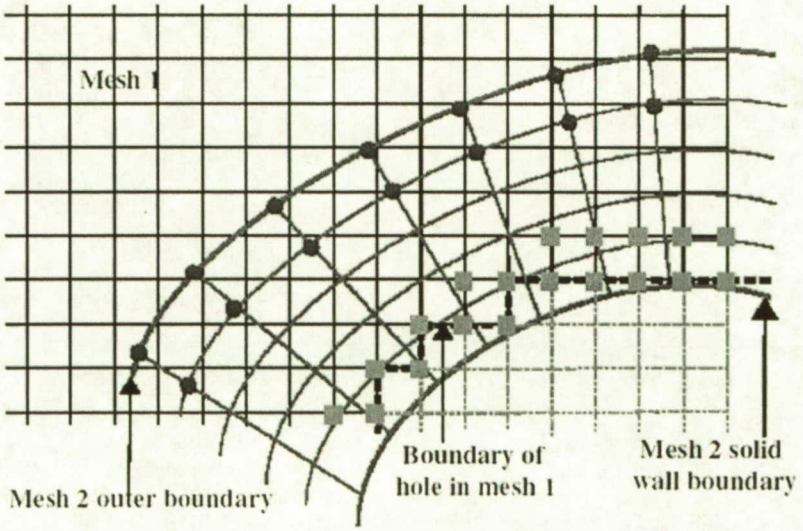

Fig. 6 Illustration of intergrid communication and interpolation in the PEGASUS code (adapted from Rogers et al. 2003)

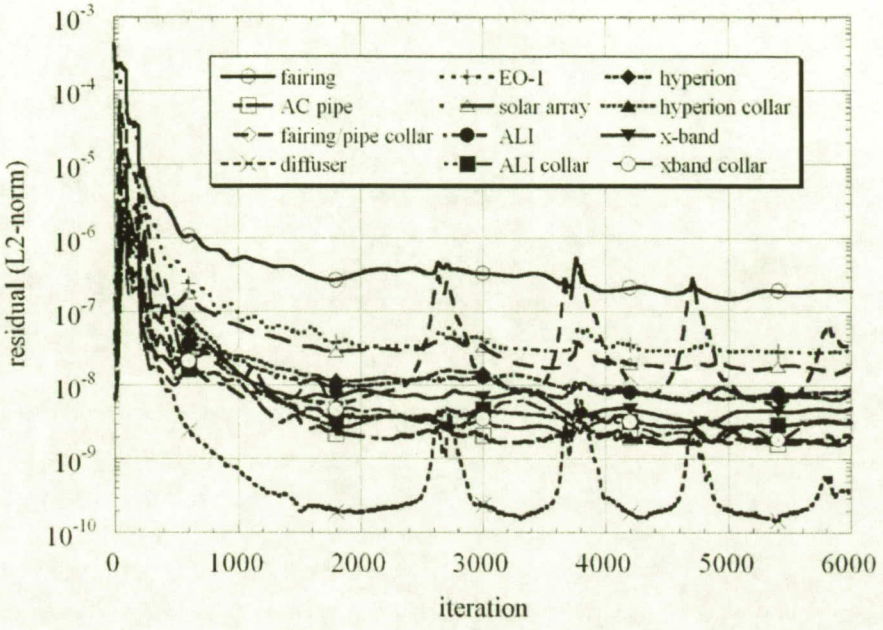

Fig. 7 Residual convergence history

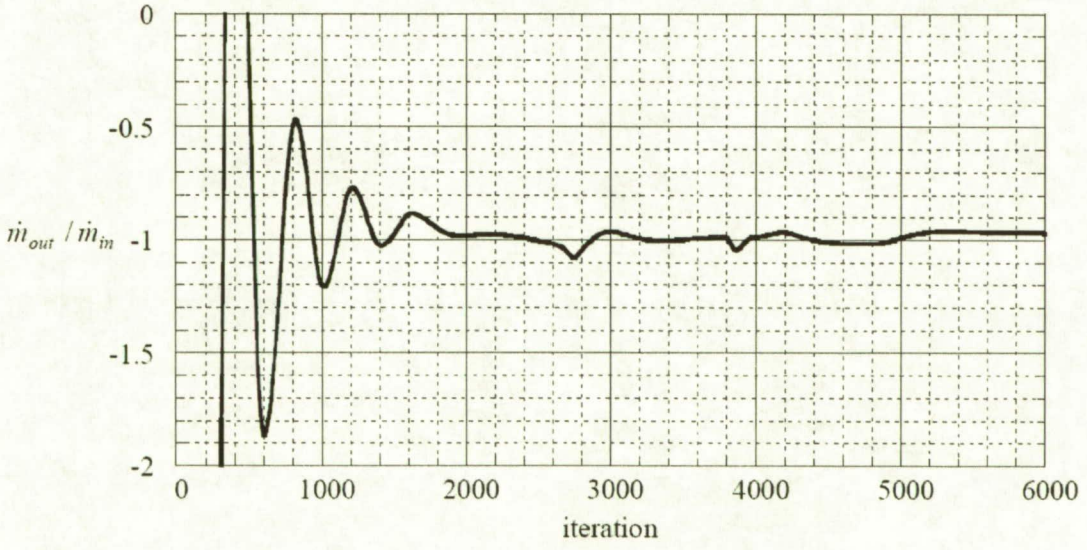

Fig. 8 Mass flow rate convergence history

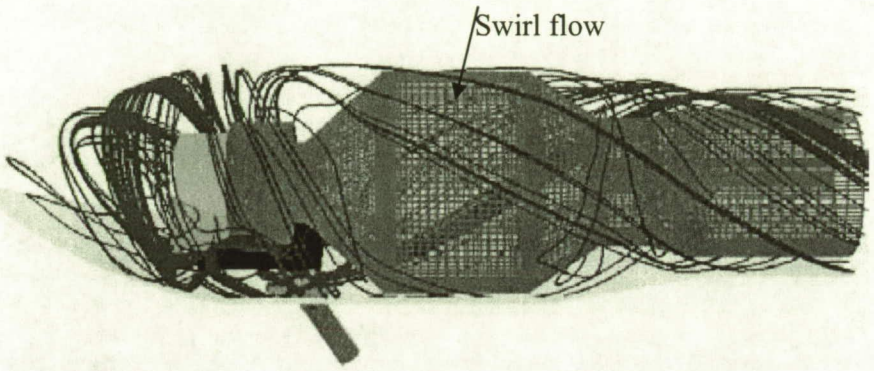

Fig. 9a Streak lines emanating from the pipe/fairing collar

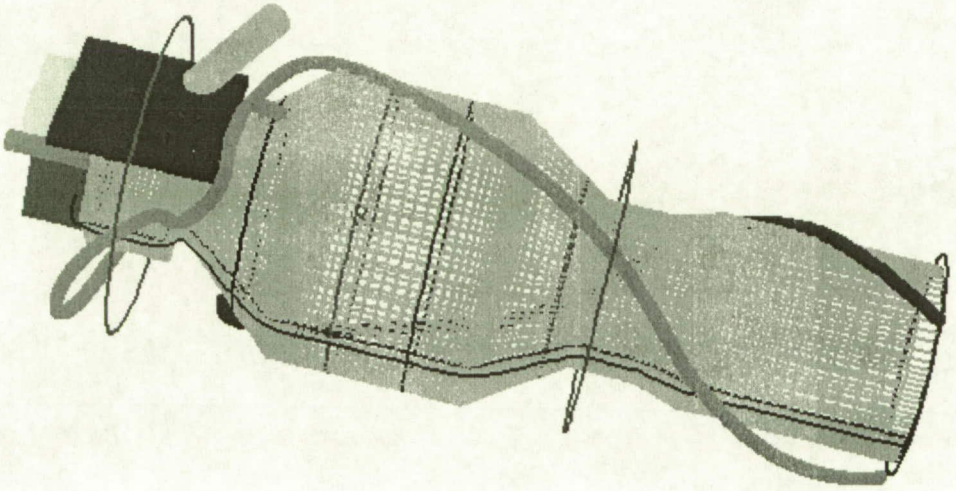

Fig.9b Typical source streak lines

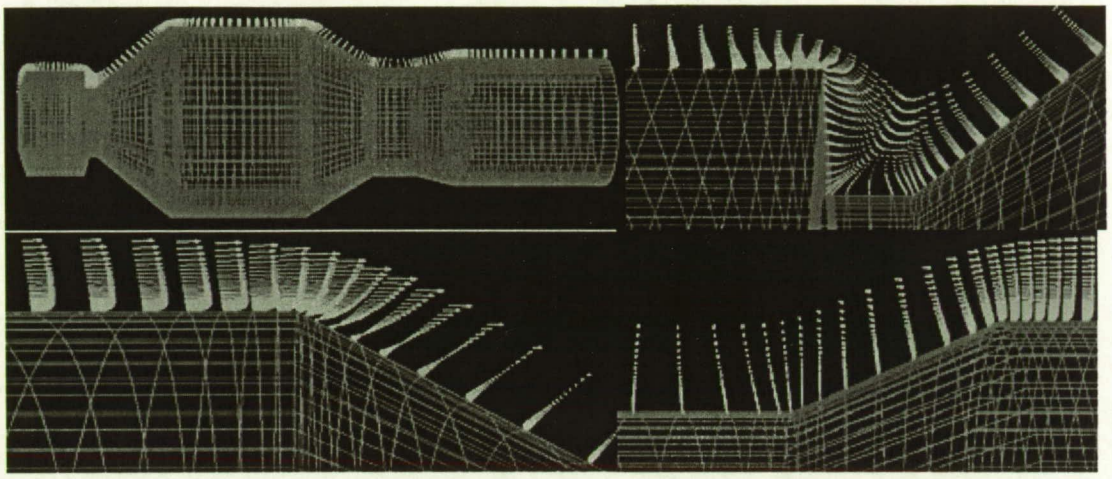

Fig. 10a Velocity vectors on EO-1

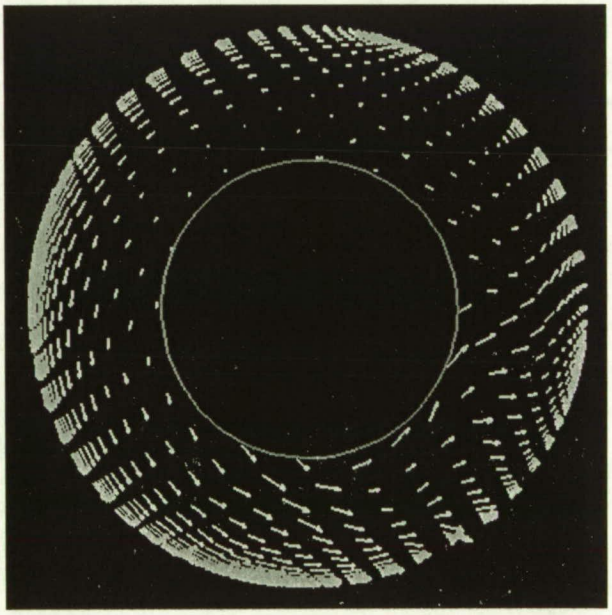

Fig. 10b Velocity vectors in the cross sectional plane of the fairing just downstream of the hexagonal structure

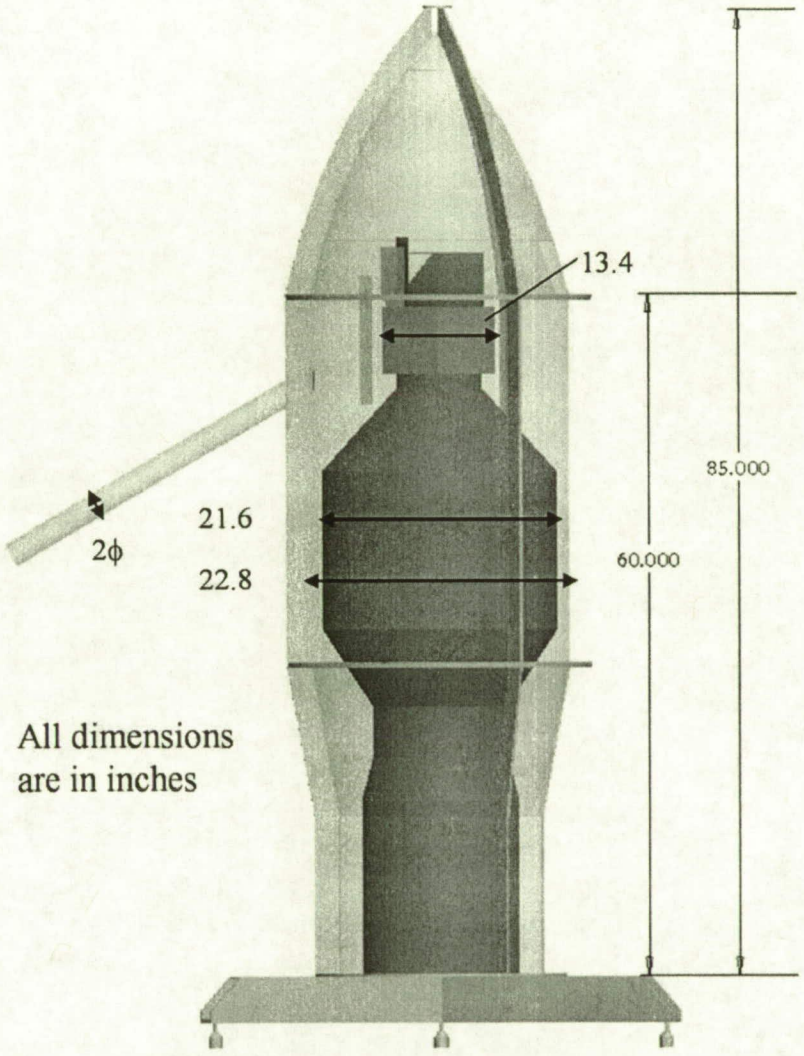

Fig. 11 Schematic of the payload/fairing test section (1/5 scale model)

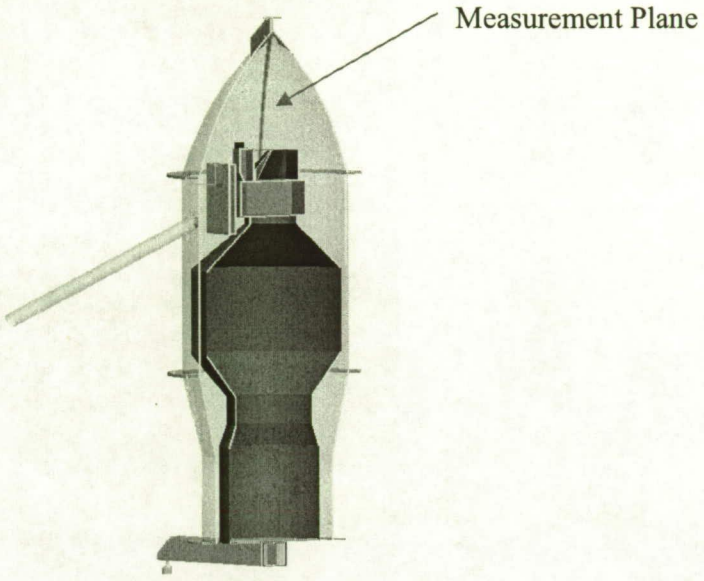

(a)

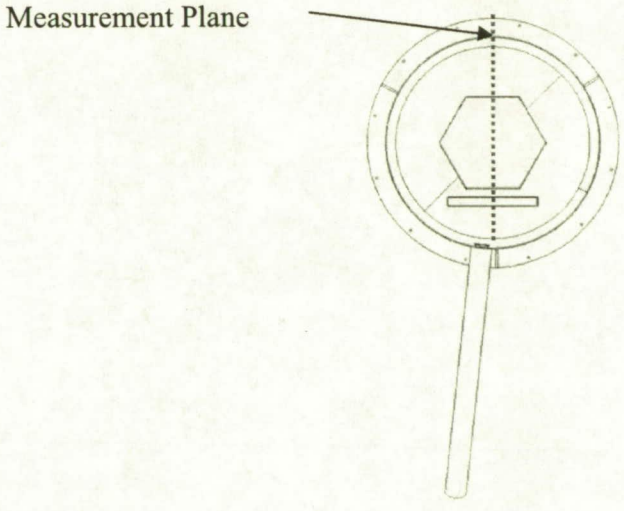

(b)

Fig. 12 LDV Measurement plane Location: a)side view and b) plan view

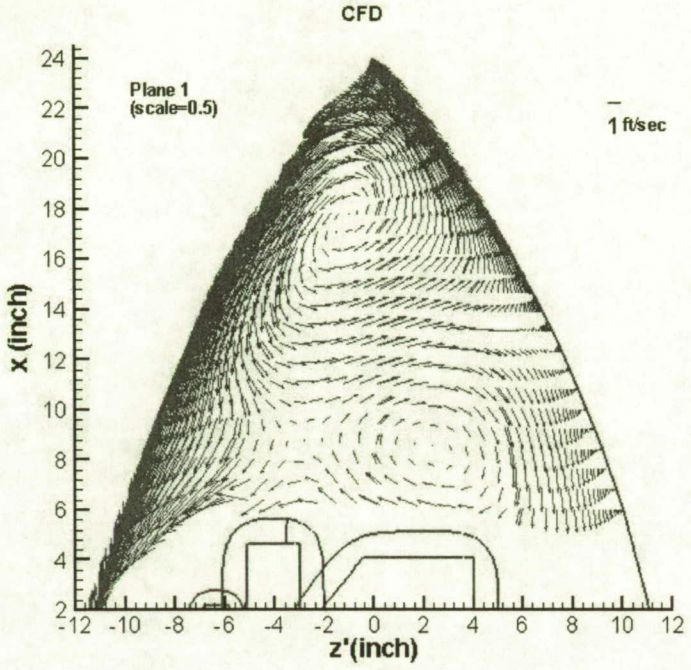

(a)

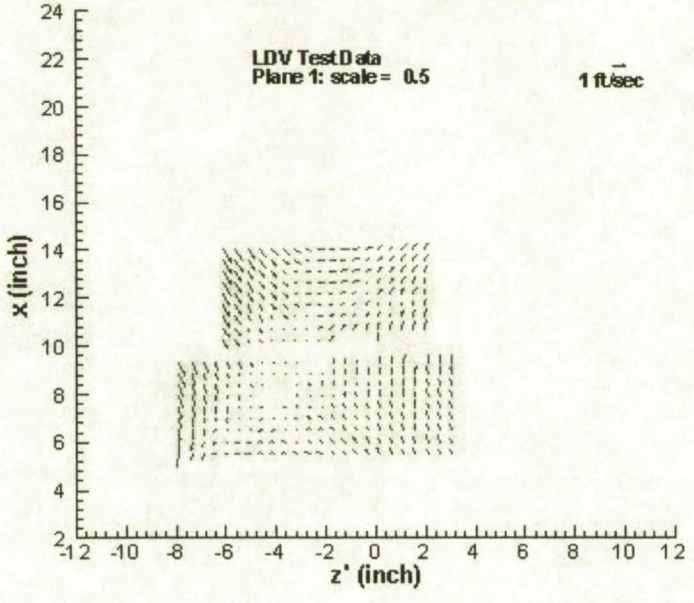

(b)

Fig. 13 Velocity vectors in the measurement plane (a) CFD (b) LDV data.

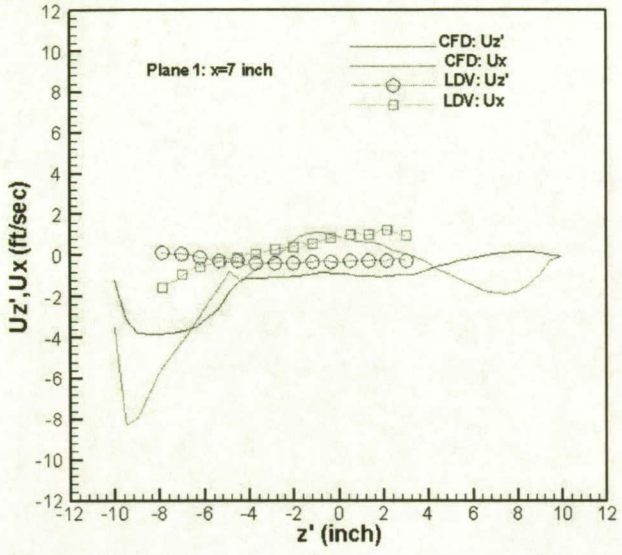

(a)

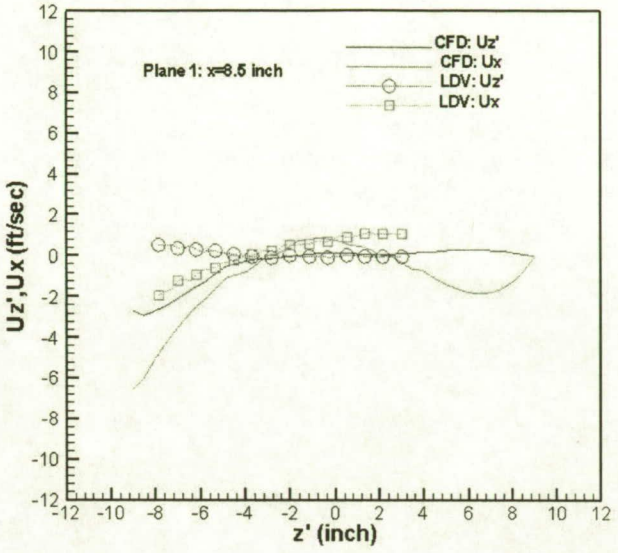

(b)

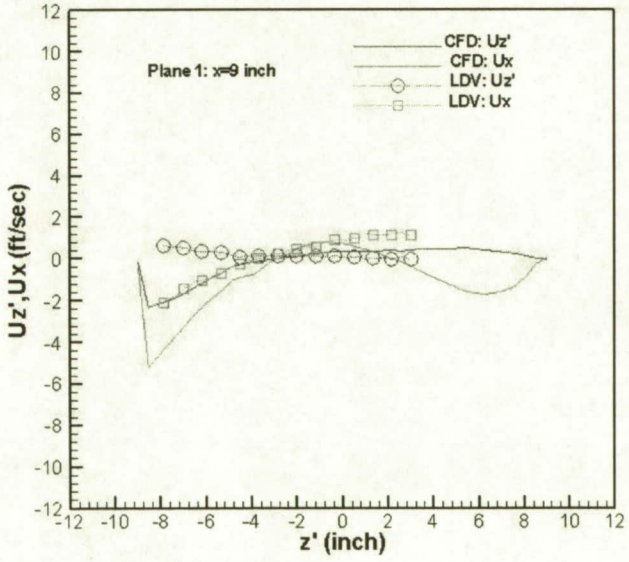

(c)

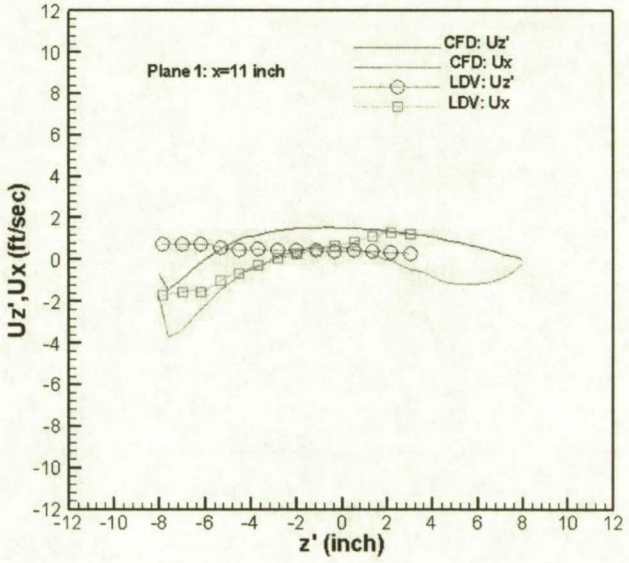

(d)

Fig. 14 Velocity profiles at constant x.

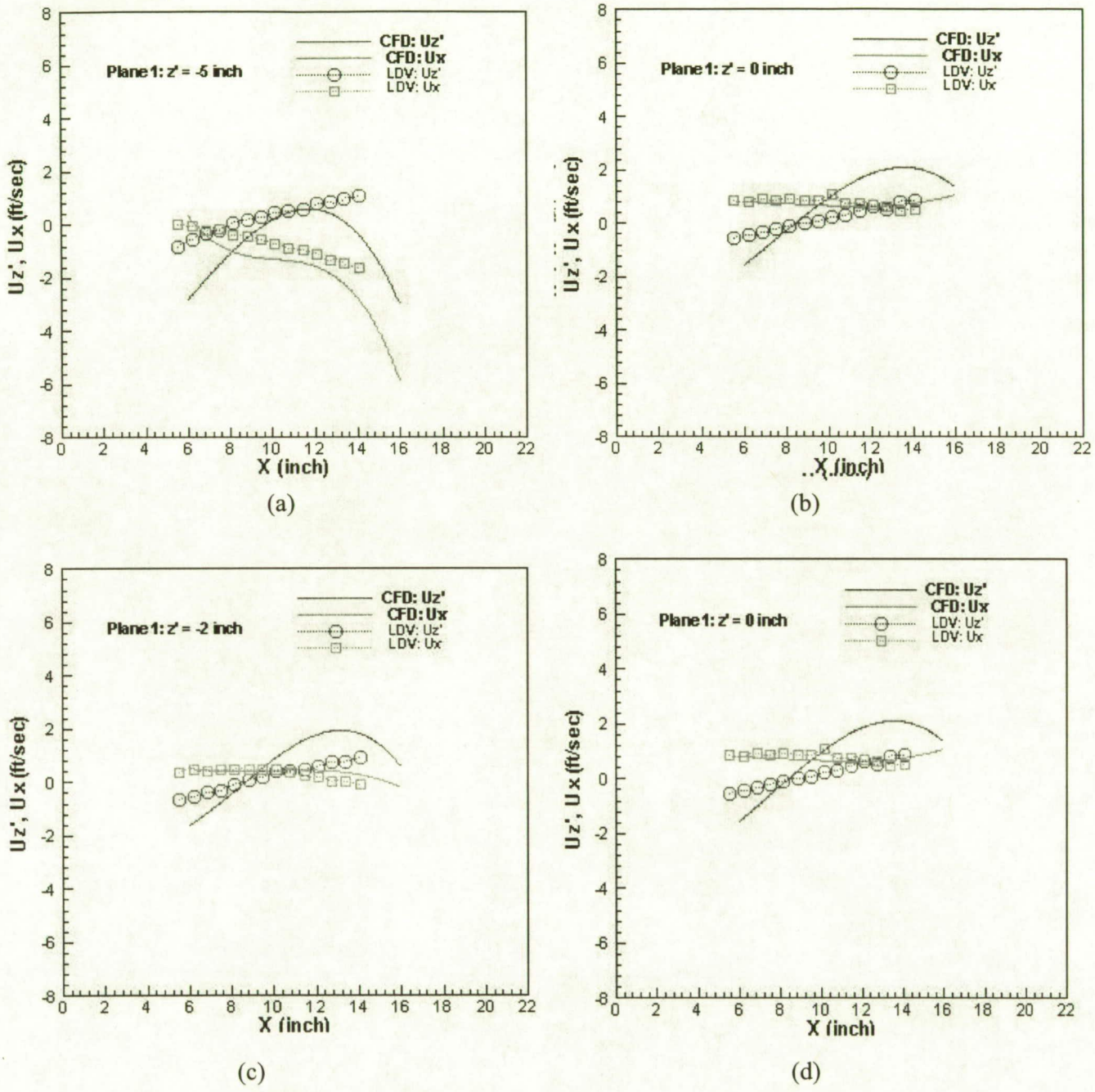

Fig. 15 Velocity profiles at constant z'.

REPORT DOCUMENTATION PAGE

Form Approved
OMB No. 0704-0188

1. REPORT DATE *(DD-MM-YYYY)*	2. REPORT TYPE	3. DATES COVERED *(From - To)*
	Journal Article	

4. TITLE AND SUBTITLE
An Application of Overset Grids to Payload/Fairing Three-Dimensional Internal Flow CFD Analysis

5a. CONTRACT NUMBER
NAS10-03006

5b. GRANT NUMBER

5c. PROGRAM ELEMENT NUMBER

6. AUTHOR(S)
M. Kandula
R. Nallasamy
P. Schallhorn
L. Duncil

5d. PROJECT NUMBER

5e. TASK NUMBER

5f. WORK UNIT NUMBER

7. PERFORMING ORGANIZATION NAME(S) AND ADDRESS(ES)
ASRC Aerospace
ASRC-3
Kennedy Space Center, FL 32899

8. PERFORMING ORGANIZATION REPORT NUMBER

9. SPONSORING/MONITORING AGENCY NAME(S) AND ADDRESS(ES)
National Aeronautics and Space Administration
VA-H3
Kenndey Space Center, FL 32899

10. SPONSORING/MONITOR'S ACRONYM(S)
NASA KSC

11. SPONSORING/MONITORING REPORT NUMBER

12. DISTRIBUTION/AVAILABILITY STATEMENT

13. SUPPLEMENTARY NOTES

14. ABSTRACT
The application of overset grids to the computational fluid dynamics analysis of 3-D internal flow in the payload/fairing of an expendable launch vehicle is described. In conjuction with the overset grid system, the flowfield in the payload/fairing configuration is obtained withthe aid of OVERFLOW Navier-Stokes code. The solution exhibits a highly 3-dimensional complex flowfield with swirl, separation, and tortices. Some of the computed flow features are compared with the measured Laser-Doppler Velocimetry (LDV) data on a 1/5th scale model of the payload fairing configuration. The counter-rotating vortex structures and the location of the saddle point predicted by the CFD analysis are in general agreement with the LDV data. Comparisons of the computed (CFD) velocity profiles on horizontal and vertical lines in the LDV measurement plane in the faring nose region show reasonable agreement with the LDV data.

15. SUBJECT TERMS
chimera overset grids, payload fairing, turbulence models, Navier-Stokes solutions, internal flow

16. SECURITY CLASSIFICATION OF:			17. LIMITATION OF ABSTRACT	18. NUMBER OF PAGES	19b. NAME OF RESPONSIBLE PERSON
a. REPORT	b. ABSTRACT	c. THIS PAGE		26	Max Kandula
					19b. TELEPHONE NUMBER *(Include area code)* (321) 867-4456